Development and Characterization of a New Solar Ultraviolet-B Irradiance Detector

B. K. DICHTER, A. F. BEAUBIEN, AND D. J. BEAUBIEN

Yankee Environmental Systems, Inc., Turners Falls, Massachusetts

(Manuscript received 2 October 1991, in final form 22 July 1992)

ABSTRACT

Characteristics of an instrument for measuring solar ultraviolet-B irradiance are presented together with a description of the instrument. The instrument measures direct and scattered broadband ultraviolet irradiance (wavelengths between 280 and 330 nm) from the hemisphere of the sky. Measurement technique employs colored glass filters in combination with a fluorescing ultraviolet-sensitive phosphor. Thermal regulation is used to significantly reduce measurement errors introduced by changes in ambient temperature.

1. Introduction

The discovery of substantial depletions of the Antarctic stratosphere ozone layer (Farman 1985) and subsequent observations of ozone depletion in the Arctic regions have made monitoring global ultraviolet radiation levels an urgent and important task. There have been indications that ultraviolet-B (UV-B, 280–320 nm) flux reaching the surface has increased slightly in the last decade. Blumthaler and Ambach (1990) report that the UV-B irradiance increased by about 1% per year in the Swiss Alps. However, it is difficult to extend the validity of this measurement to more urban areas, with their higher local concentrations of UV-B absorbers, aerosols, and tropospheric ozone. The measurement of long-term trends of UV-B levels across the surface of the earth remains an open experimental problem, awaiting the establishment of widespread UV-B monitoring networks and improvements in the current measurement technology.

The development of the instrument described in this paper was prompted by the recognition of the need for a modest-cost broadband instrument that could be used in networks throughout the world to measure global solar UV-B irradiance. Spectroradiometers are required to establish baseline data for the networks and serve as reference instruments, but the expense and complexity of these instruments make them impractical for widespread use. A simpler, less expensive instrument can be used to supplement the spectroradiometer measurements and extend the geographical range of UV-B monitoring coverage.

Measurement of solar UV-B irradiance with conventional optical detection schemes is difficult because the amount of energy present in the UV-B region is less than 0.1% of the total amount of energy in the visible portion of the solar spectrum. In addition, most photodetectors have their peak responses in the visible wavelengths rather than in the ultraviolet portion of the spectrum. Since the 1930s a number of techniques, including chemical and radiometric (Coulson 1975), have been tested in an effort to measure solar UV-B irradiance. The current generation of broadband UV-B detectors is based on an extension of the work of Robertson (1972), who implemented the use of a UV-B sensitive fluorescent phosphor as the active element of his detector. Further refinements to the original Robertson meter were made by Berger (1976). Some present day versions of this instrument are referred to as Robertson–Berger meters, or simply R–B meters.

The original Robertson design proved to be successful. For the first time it allowed the use of an inexpensive instrument to make quantitative measurements of solar UV-B-radiant exposure. The instrument was adopted for use in several monitoring networks, which now have a database of nearly 15 years in duration. Based on the success of the Robertson design, we sought to build an improved version of the instrument that reduces or eliminates the instrumental measurement errors. The most significant error of the current R–B meters is due to dependence of the output signal on ambient temperature; the size of the effect on the signal is 1% $°C^{-1}$.

The goal of our program was the development of an instrument that would make accurate quantitative measurements of global solar UV-B irradiance and effective erythemal irradiance. We determined that the new instrument must meet some basic criteria

1) The instrument should employ up-to-date high-reliability components to assure maximum reliability in the field.

2) Procedures for depositing the fluorescent phosphor and selection and characterization of the colored

Corresponding author address: Dr. B. K. Dichter, Yankee Environmental Systems, Inc., 101 Industrial Road, P.O. Box 746, Turners Falls, MA 01376.

glass filters must be highly standardized and demonstrably repetitive.

3) Errors due to the thermal dependence of the output of the instrument must be substantially reduced and, preferably, eliminated.

4) Procedures for establishing the cosine, spectral, absolute, and thermal characteristics for the instrument must be standardized, transferable, and traceable to the National Institute of Standards and Technology (NIST).

2. Principle of operation

The instrument uses a UV-B-sensitive fluorescing inorganic phosphor—magnesium tungstate ($MgWO_4$). This material absorbs incident UV-B light and reemits it as visible light (predominantly green). The emitted light is then measured by a solid-state photodiode. Colored glass filters are used to absorb visible light before it can reach the photodetector. A block diagram of the instrument is shown in Fig. 1, while the global solar irradiance and the spectral properties of the optical elements of the instrument are shown in Fig. 2.

Solar radiation (Fig. 2a), both direct and scattered, passes through the UV-transmitting weather dome (Schott WG 280 glass). The first active element of the instrument is the prefilter, a 25-mm diameter, 1.6-mm-thick UV-transmitting black glass (Schott UG 11). This filter passes 80% of the incident UV-B light and has only one weak transmission band in the visible region, around 750 nm (Fig. 2b). A mixture of UV and red light, transmitted through the prefilter, strikes the $MgWO_4$ phosphor. The red light is scattered by the phosphor, while the UV-B light is absorbed and reemitted as visible (Fig. 2c). A 25-mm diameter 2.5-mm-thick green glass (Corning 4010) postfilter passes the fluorescent light from the phosphor while blocking the red light transmitted by the black glass (Fig. 2d). The intensity of the fluorescent light is measured by a solid-state photodiode (Hamamatsu G1117). This photodetector, utilizing gallium arsenide phosphide (GaAsP) technology, has its peak spectral response in the region of green light, dropping off rapidly at the longer wavelengths (Fig. 2e), thus further reducing the instrumental response to red light. A thermally stable transimpedance amplifier raises the output current level of the photodiode and drives a line amplifier to provide a low impedance 0–5-V dc output signal. Finally, since the performance of the critical components of the detection system—phosphor and photodiode—are temperature dependent, the instrument design incorporates a common, thermally controlled holder for these elements. Both the amplifier and thermal control circuits are located inside the detector housing.

3. Phosphor considerations

The choice of the UV-B sensitive phosphor and the technique for its deposition are the critical elements in the design of this instrument. We have reexamined the desirability of using Robertson's choice of $MgWO_4$ asthe phosphor, since this is a relatively old phosphor and many new materials have been developed as a result of the growth of the fluorescent tube industry over the past three decades. Some of the newer phosphors with similar excitation spectra do offer better quantum efficiencies or better temperature independence. In view of the fact that the large amount of data collected on solar UV-B radiation levels (Scotto and Fears 1977;

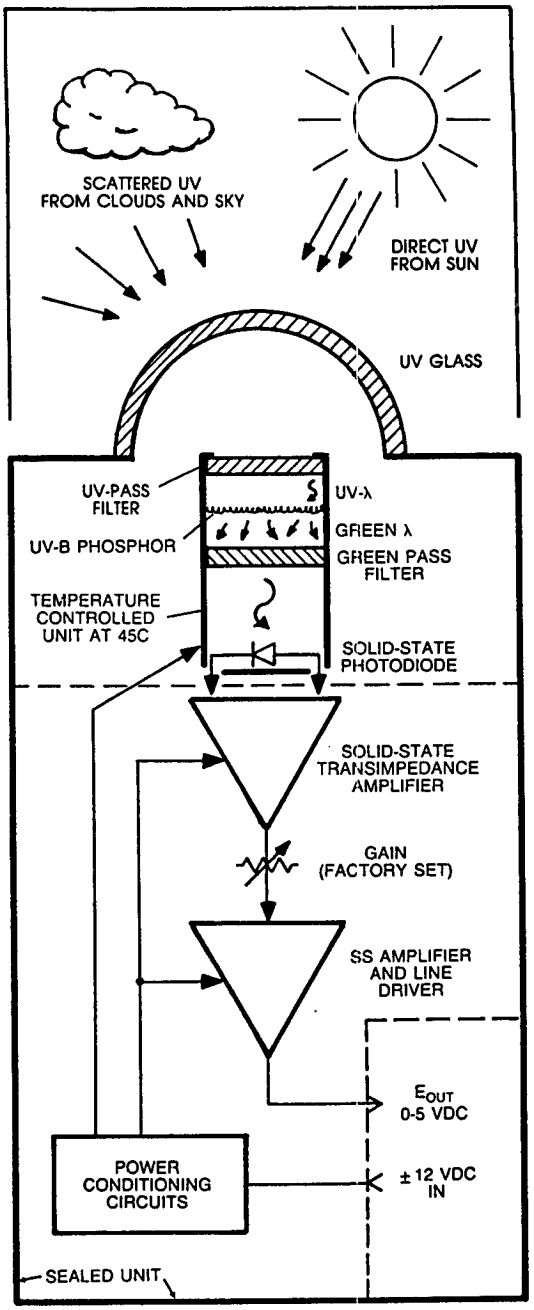

FIG. 1. Schematic block diagram of the instrument.

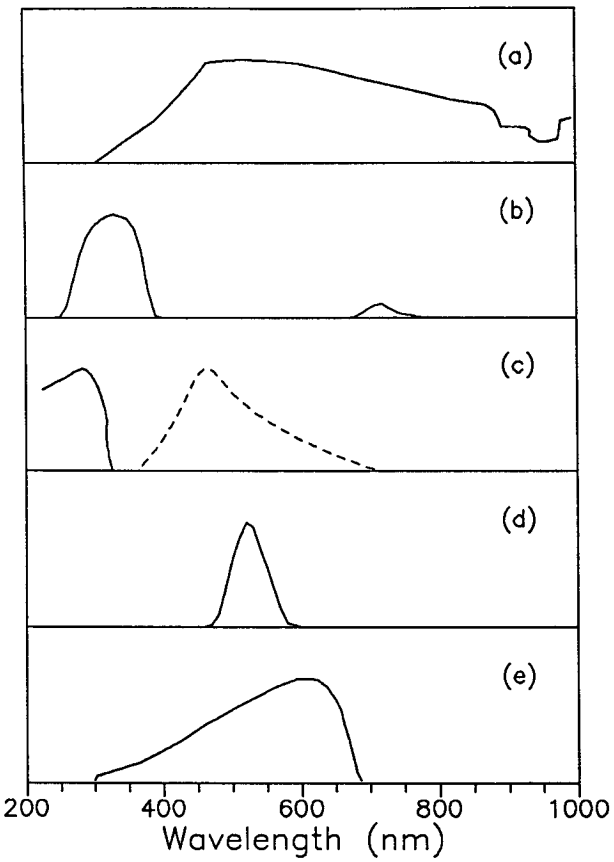

FIG. 2. Linear scale plots of key spectral functions: (a) typical global solar spectral irradiance at the earth's surface (maximum plotted value is 0.8 W m^{-2} nm^{-1}); (b) transmission curve of the UG-11 filter (maximum plotted value is 80%); (c) relative excitation (solid line) and emission (dashed line) spectra of the $MgWO_4$ phosphor; (d) transmission curve of the Corning 4010 filter (maximum plotted value is 80%); and (e) spectral response of the GaAsP photodiode (maximum plotted value is 0.2 A W^{-1}).

DeLuisi and Harris 1983) has been obtained using $MgWO_4$-based detectors, we concluded that it was not advantageous at this time to change this component of the instrument. Future development of phosphors, and of standardized procedures of calibrating UV-B detectors, may lead to the adoption of a different phosphor.

In order to provide data of the quality required to determine the earth's UV-B climatology, the monitoring instruments must be able to function stably, without drift, for long periods of time and to have consistent and reproducible spectral, cosine, and absolute responses. For these reasons, considerable effort has been expended to establish a standard procedure for depositing a uniform, reproducible, and highly stable layer of the phosphor. A deposition procedure was obtained from a specialty cathode ray tube manufacturer, who had used the same process for nearly 30 years to produce streak camera cathode ray tubes. The phosphor used for the streak cameras was not $MgWO_4$ but a similar inorganic material. Phosphor layers that had been deposited by this process more than 30 years ago were obtained, and their condition and performance were found to be the same as those being deposited today. Using this deposition technique, we were able to produce uniform reproducible layers of $MgWO_4$ with areal densities that do not vary by more than 15%. Based on our experience with the phosphor deposition process, we believe that these layers have a high probability of maintaining their performance over many years.

The thickness of the phosphor layer must be carefully chosen to optimize the performance of the instrument. The proper thickness represents a compromise between a layer thick enough to absorb the incident UV light but thin enough to efficiently transmit the reemitted visible light out of the phosphor and into the photodetector. Although the absorption length of visible light in the phosphor is much larger than the absorption length of the UV-B, phosphor particles scatter and reflect the visible light readily and direct it away from the photodiode. After considerable testing, we have found that a 1 mg cm^{-2} areal density layer of phosphor, with a 4-μm mean particle diameter, gives the best performance in terms of overall UV-B detection efficiency. Experimentally, we have found that phosphors with larger size particles have a lower UV detection efficiency and therefore require thicker layers to be deposited.

The thickness of the deposited layers cannot vary significantly from unit to unit because the spectral response of a phosphor layer depends on its thickness. For example, increasing the layer areal density from 1 to 2 mg cm^{-2} shifts the peak of the phosphor excitation spectrum by 2 nm toward the longer wavelengths. The phosphor layers obtained using our deposition procedure are uniform to within 15%, and the observed unit-to-unit variation of the position of the peak of spectral response is less than 0.5 nm (limit of our measurement system resolution). The relative spectral response curves of the units, in the region of 280–330 nm, are also identical to better than 0.5 nm.

4. Choice of photodetector

Earlier R–B meters that have evolved from the original Robertson design employ a vacuum photodiode (1P39). The large size and mounting scheme of this detector forces the optical filters to be approximately 75 mm in diameter, making thermal stabilization difficult to incorporate. Several significant improvements in the new instrument resulted from replacing the 1P39 vacuum photodiode with a solid-state GaAsP photodiode. This device has its peak spectral response near the green region and is therefore well matched to detect the emissions from the $MgWO_4$. It is also, according to manufacturer's specifications, not sensitive to red

light transmitted by the UG 11 glass (see Fig. 2e). The filter–photodetector combination used in the instrument renders it "solar blind," suppressing the visible response at least five orders of magnitude.

In addition to the excellent spectral match of the GaAsP photodiode to the filter system, the device is physically small in size, only 14 mm in diameter (TO-8 electronic package). This allows the glass filters to be reduced to only 25.4 mm in diameter, resulting in a considerable reduction in the cost of these components. The overall reduction in size for the critical detector components lowers their thermal mass to the point where thermal stabilization can be easily accomplished.

5. Detailed instrument description

A cross section of the detector sensor head is shown in Fig. 3. The upper ring is fabricated from Delrin to minimize thermal conduction to the cast aluminum body of the instrument. The UG-11 filter with the phosphor layer deposited on its rear surface, the Corning 4010 green filter, and the GaAsP photodiode are mounted within an aluminum bobbin to ensure that these components remain at a common temperature. The bobbin is wrapped with a resistive foil heater, and is in good thermal contact with a control thermistor. An electronic circuit is used to thermally regulate the entire assembly, which is held at a constant temperature of +45°C. This temperature is above the operating temperature of the instrument under normal field conditions. The control temperature can be higher (lower) than +45°C if required in high (low) ambient temperature installations. A second (monitor) thermistor allows the bobbin temperature to be measured independently if desired.

If an instrument operates in an environment where the ambient temperature is above a preset control temperature, the thermal control circuit will shut down until the sensor head temperature drops below the control temperature. During that time, the sensor head temperature will track the ambient temperature and the instrument output signal will need to be corrected. Temperature corrections are discussed in section 6. The sensor head temperature can be obtained from the monitor thermistor readings.

The amount of power required to maintain the bobbin assembly at +45°C from an ambient temperature of −40°C was measured to be approximately 5 W (0.4 A at 12 V). At a nominal ambient temperature of +20°C, the power required to maintain the bobbin at the control temperature is about 1.3 W. The electronic thermal regulation circuit is designed to provide up to 0.5-A current to the heater. The time required for the bobbin to reach the control temperature is typically less than 2 min from a turn-on temperature +20°C, increasing to 12–15 min when the starting temperature is −40°C. The warm-up times become important in installations where power availability is limited, and the instrument is operated on a cyclical basis.

The solid-state GaAsP photodiode permits the use of a transimpedance amplifier. This allows a high-level low-impedance output signal, 0–5 V full scale, to be developed directly at the sensor. The transimpedance amplifier and line driver operate from ±12-V dc power supply and require 0.24 W. It should be noted that the response time of the phosphor (ms) is much faster than that of the changes in environmental UV-B irradiance. The overall response of the instrument is governed by the value of the feedback capacitor in the transimpedance amplifier. We have found that a response time

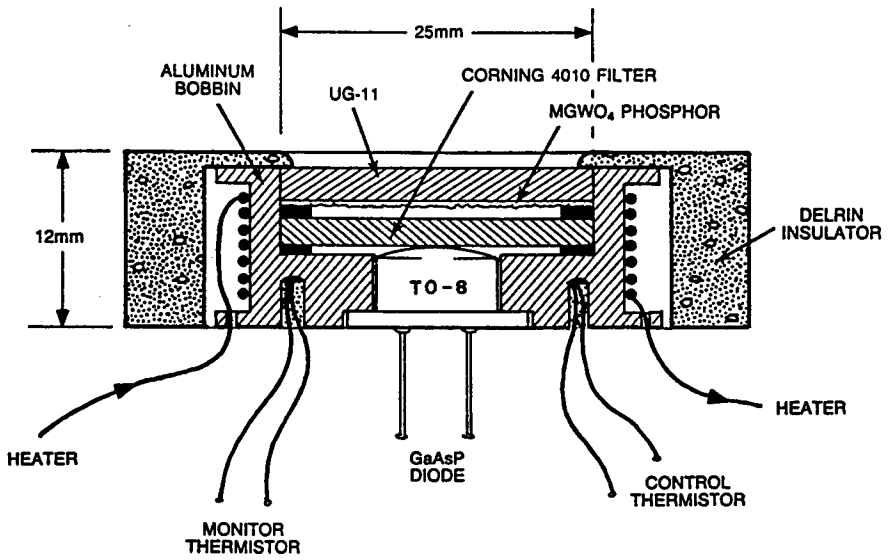

FIG. 3. Detailed cross section of the instrument sensor head.

on the order of 0.1 s is an optimal choice for the instrument, enabling it to follow changes in UV-B due to cloud movements without introducing electronic noise.

6. Instrument performance

a. Temperature effects on spectral response

The spectral response of the instrument is determined on the short wavelength side by the weather dome (WG 280 glass), which absorbs light with wavelengths shorter than 280 nm. Since solar radiation with shorter wavelengths does not penetrate to the surface of the earth, this is not a limitation for a meteorological instrument. (Should it be required to measure the solar flux below 280 nm, a quartz dome can be substituted for the WG 280 dome.) On the long wavelength side, the spectral response of the instrument is determined by the excitation spectrum of the $MgWO_4$ phosphor.

The excitation and emission properties of the phosphor as a function of temperature are complex (Butler 1982) and must be carefully considered in the design of the instrument. Excitation of the phosphor occurs when one of the valence electrons in the $MgWO_4$ solid absorbs a UV-B photon and is promoted from the ground state to the first excited state. The electron then undergoes interactions with the solid, losing some of its energy. Finally, the electron emits a lower-energy (longer wavelength) photon, indicating that it lost energy to the solid, and returns back to the ground state.

The effects of increasing temperature on this process are twofold: 1) the effective ground state–excited state energy gap decreases in magnitude and 2) deexcitation modes, other then photon emission, become increasingly accessible to the excited electron. The result of the decreasing energy gap is to allow lower-energy photons to excite the phosphor, thus shifting the excitation curve toward longer wavelengths. The effect of competing deexcitation modes is to decrease the probability of reemission of (green) light by the phosphor, thus lowering its efficiency as a converter of UV-B to green light.

The absolute spectral response of the instrument was measured using the experimental arrangement shown in Fig. 4. A 150-W xenon arc lamp was used as the UV light source. Most of the visible light in the beam was blocked by placing a UG-11 glass filter as the output of the lamp. The filtered light illuminated a holographic grating monochromator, which was used to select a narrow range of wavelengths (2 nm wide) to pass through its exit slits. The monochromatic light was focused into a 25.4-cm-diameter integrating sphere. A calibrated, NIST-traceable, reference detector was mounted in one sphere port while the UV-B instrument was mounted in a second port.

The measurement procedure was performed using a computer-based data acquisition system. The monochromator was stepped through the calibration wavelength range, 270–400 nm, in 2-nm increments. At each wavelength under study, the reference detector and the instrument outputs were recorded. After the spectral scan was completed, the absolute sphere wall irradiance at each wavelength was calculated from the reference detector measured values. The irradiances and instrument output readings were then used to obtain the absolute spectral response.

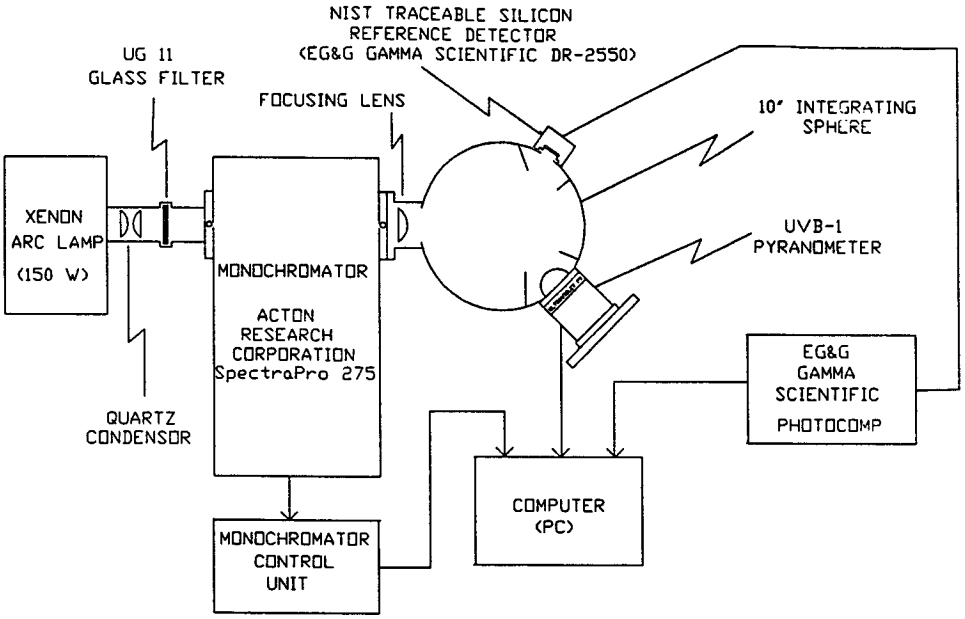

FIG. 4. Schematic diagram of the experimental arrangement used to measure absolute spectral response of the instrument.

Spectral response curves taken with the instrument held at three different temperatures are shown in Fig. 5. (The curves have been normalized to the peak spectral response at 0°C.) The simultaneous action of both temperature effects is evident. As the temperature increases, the absolute efficiency of the phosphor decreases and the spectral response shifts to longer wavelengths. The result of this behavior of the phosphor is that the thermal variation of the instrument output depends on the spectrum of incident radiation. When a Xe arc lamp, with a spectrum slowly varying with wavelength in the UV region, is used to illuminate the instrument, the shift in spectral response is not important and the loss of efficiency dominates. We have found that in the ambient temperature range of −20° to +40°C, the change in the instrument output when illuminated with a Xe arc lamp is about $-0.5\%\,°C^{-1}$. Solar irradiance, on the other hand, increases exponentially with wavelength in the UV-B region, and the decrease in efficiency is not as important as the shift in the spectral response, which allows the far more numerous lower-energy photons to excite the phosphor. The change in output for an instrument exposed to sunlight was measured to be $+1.0\%\,°C^{-1}$. These results are in good agreement with values published by Blumthaler and Ambach (1986) for a Robertson–Berger meter.

b. Cosine error

The broadband UV-B detector is in a class of optical instruments designed to measure the amount of radiation falling on a plane surface. An ideal instrument of this type, with a sensitive area A, responds to light incident at an angle θ with an effective area of $A\cos(\theta)$. Cosine error is any deviation from $\cos(\theta)$ behavior. This error is generally caused by two factors: 1) rapid changes in surface reflectance for near-grazing light rays, and 2) for values of θ close to 90°, parts of the sensitive area may be obstructed by the edges of the instrument. The ratio of the measured instrument response to the ideal response as a function of angle of incidence of light, $\delta(\theta)$, is listed in the second column of Table 1.

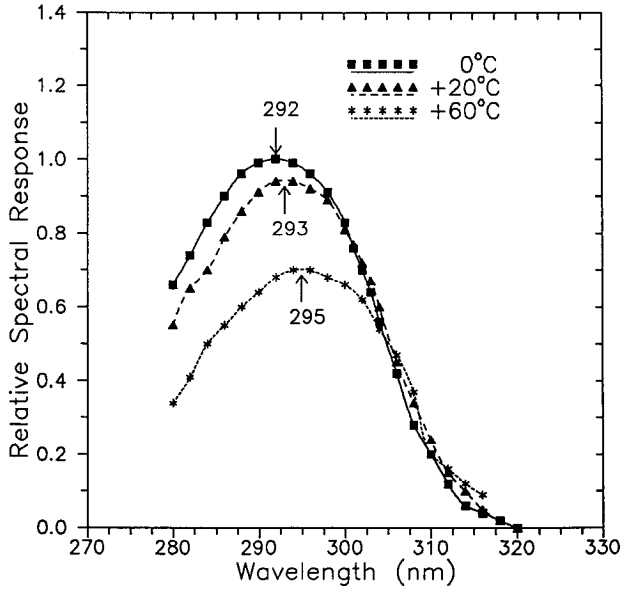

FIG. 5. Relative instrumental spectral response curves at three temperatures. Arrows indicate wavelength of peak spectral response.

The effective cosine error of the instrument is not described by the function $\delta(\theta)$, because solar UV irradiance at the surface of the earth has both a directly transmitted and a scattered component. Cosine error due to the direct component is given by $\delta(\theta)$, but the cosine error due to the scattered component must be evaluated by integrating over the entire hemisphere of the sky. The ratio of intensities of the two components varies strongly with solar zenith angle. For example, for large zenith angles, UV-B irradiance is nearly all scattered. In this case, the cosine error approaches the scattering component cosine error and becomes nearly independent of the value of δ for the actual zenith angle.

The effective cosine correction can be calculated as follows. If we make the reasonable assumption that diffuse UV-B light flux is uniform over the sky hemisphere, then the effective global irradiance, G_i, as a function of solar zenith angle, θ_s, measured by an instrument with an ideal cosine response is given by

$$G_i(\theta_s) = G_t(\theta_s)\cos(\theta_s) + G_d(\theta_s), \qquad (1)$$

where $G_{t(d)}$ is the transmitted (diffuse) irradiance. In turn, $G_{t(d)}$ can be written as an integral over the wavelength λ:

$$G_{t(d)}(\theta_s) = \int g(\lambda)e_{t(d)}(\lambda, \theta_s)d\lambda, \qquad (2)$$

where $e_{t(d)}(\lambda, \theta_s)$ is the transmitted (diffuse) solar spectral irradiance and $g(\lambda)$ is the instrument spectral response. The physical detector will measure an effective irradiance G_m:

$$G_m(\theta_s) = K[\delta(\theta_s)\cos(\theta_s)G_t(\theta_s) + \epsilon G_d(\theta_s)], \qquad (3)$$

with

$$\epsilon = 2\int_0^{\pi/2} \delta(\theta)\sin(\theta)\cos(\theta)d\theta, \qquad (4)$$

where K is a calibration constant. Evaluating Eq. (4) with the measured instrumental values for $\delta(\theta)$ yields $\epsilon = 0.93$. The cosine correction factor is the ratio G_i/G_m. In practice, the calibration constant K is fixed by the calibration requirement that at an arbitrarily chosen zenith angle of approximately 30° the instrument readout must agree with a known solar spectrum. This forces the cosine error to be zero at the calibration angle.

TABLE 1. Listing of the $\delta(\theta)$ function values and the cosine, erythemal, and total UV-B instrumental correction factors as a function of solar zenith angle.

Zenith angle (θ)	$\delta(\theta)$	Clear-sky correction factors		
		Cosine	Erythemal	Total UV-B
0	1.00	0.996	1.062	0.959
5	1.00	0.996	1.060	0.960
10	1.00	0.997	1.055	0.964
15	1.00	0.997	1.046	0.969
20	1.00	0.998	1.034	0.977
25	1.00	0.999	1.019	0.987
30	1.00	1.000	1.000	1.000
35	1.00	1.001	0.978	1.015
40	1.00	1.003	0.953	1.032
45	1.00	1.004	0.925	1.052
50	0.98	1.011	0.900	1.077
55	0.96	1.018	0.873	1.100
60	0.92	1.026	0.852	1.122
65	0.88	1.031	0.838	1.128
70	0.79	1.037	0.841	1.112
75	0.67	1.035	0.872	1.058
80	0.53	1.027	0.926	0.969
85	0.36	1.024	1.003	0.873

Calculated clear-sky cosine correction factors are listed in column 3 of Table 1. Solar UV irradiances were calculated using the atmospheric transmission model of Green et al. (Green 1974). Note that the correction factor is 1.000 at $\theta_s = 30°$ as a result of the calibration procedure. The effective cosine error is less than 1% out to zenith angles of 50° and reaches a maximum of 3.8% at 70°. Beyond 70°, the cosine error decreases because the transmitted component of the irradiance becomes vanishingly small and the cosine error associated with this term goes to zero. For 100% overcast conditions (no transmitted irradiance component) the calculated cosine correction factor relative to the clear-sky $\theta_s = 30°$ factor has a value of 1.02, independent of solar zenith angle.

It should be noted that if the quantity of interest is the summed daily radiant exposure to UV-B radiation for locations in the low and midlatitudes, the effective cosine error will be small (less than 1% in the spring and summer). This is because the bulk of the dose will be accumulated while the sun is high in the sky (small values of θ_s) and, consequently, the cosine error is at its minimum.

c. *Spectral error*

Output signal of an instrument is proportional to the convolution of the instrument spectral response and the spectrum of incident light. Instrumental spectral error occurs when making a measurement with an instrument that has a different spectral response from a desired one; for example, making a measurement of UV-B irradiance with an instrument that has some response to UV-A light. Since the shape of the UV portion of the solar spectrum at the earth's surface changes significantly with zenith angle, the spectral error will also change with zenith angle.

The spectral response of the instrument, over nearly five orders of magnitude, is shown plotted in Fig. 6. The measurements were performed at NIST using an argon arc lamp and a double monochromator as the source of monochromatic light. Also shown in Fig. 6 is the human erythemal action spectrum (Parrish 1982).

When measuring a phenomenon characterized by a spectral function $h(\lambda)$, a combined spectral and cosine correction for the instrument can be calculated by taking a ratio of the $G_m(\theta_s)$ term and a term $H_i(\theta_s)$, which describes the effective irradiance as measured by an ideal detector with a spectral response $h(\lambda)$:

$$H_i(\theta_s) = \cos(\theta_s)H_t(\theta_s) + H_d(\theta_s). \quad (5)$$

The terms $H_{d(d)}$ are calculated by replacing $g(\lambda)$ in Eq. (2) by the desired spectral function, $h(\lambda)$. If monitoring of the total UV-B is desired, then $h(\lambda)$ must be set to unity of $280 \leqslant \lambda \leqslant 320$ nm, and to zero otherwise. If monitoring of erythemally effective radiation is required, then $h(\lambda)$ can be set to a functional fit to the erythemal spectrum.

Sets of calculated clear-sky instrument correction factors for measuring erythemally effective radiation and total UV-B radiation are listed in columns 4 and 5 of Table 1. As in the case of the cosine corrections, the correction factors are relative to a solar zenith angle of 30°. The instrument can be used to make meaningful quantitative measurements of both total UV-B irradiance and effective erythemal irradiance out to the largest zenith angles, as long as care is used and proper

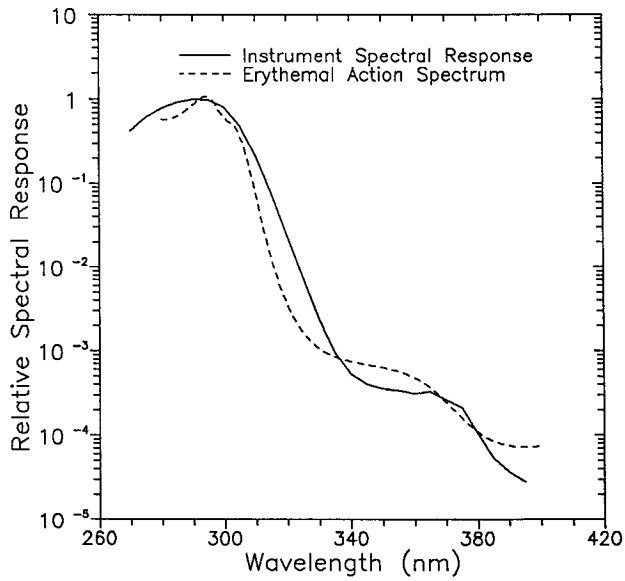

FIG. 6. Instrumental spectral response (solid line) and erythemal action spectrum (dashed line).

corrections are applied when treating large-zenith angle data.

The correction factors (relative to the clear-sky $\theta_s = 30°$ values) calculated for various solar zenith angles for 100% overcast conditions do not differ from the corresponding clear-sky values by more than 4% for effective erythemal irradiance and by more than 2% for total UV-B irradiance. The combination of large size of the diffuse component of the UV-B irradiance and the fact that our instrument measures global broadband UV-B irradiance makes it relatively immune to measurement errors caused by changing cloud conditions.

7. Conclusions

We have designed, built, and tested an instrument suitable for reference grade measurements of broadband UV-B solar irradiance. The instrument features several improvements over previous meters of this type. Most notably, the instrument is free of temperature-induced errors and can be manufactured with a high degree of uniformity from unit to unit, rendering the design suitable for network applications.

Acknowledgments. Sincere thanks are due to our colleagues at EG&G who have made many helpful comments over the years on the design of the instrument, especially Dr. Bruno Finnocchio and Mr. Robert Ruff. This work owes much to the constant encouragement and enthusiasm of Dr. John DeLuisi of The National Oceanic and Atmospheric Administration, Boulder, Colorado. This work was partially funded by the United States Department of Agriculture–Small Business Innovation Research Agreement 91-33610-5951.

REFERENCES

Berger, D. S., 1976: The sunburning ultraviolet meter: Design and performance. *Photochem. Photobiol.*, **24,** 587–593.

Blumthaler, M., and W. Ambach, 1986: Measurements of the temperature coefficient of the Robertson–Berger sunburn meters and the Eppley UV-radiometer. *Arch. Meteor. Geophys. Bioklim.*, **B36,** 357–363.

——, and ——, 1990: Indication of increasing solar ultraviolet-B radiation flux in Alpine regions. *Science,* **248,** 206–208.

Butler, K. H., 1982: *Fluorescent Lamp Phosphors.* Pennsylvania University Press, 351 pp.

Coulson, K. L., 1975: *Solar and Terrestial Radiation.* Academic Press, 322 pp.

DeLuisi, J. J., and J. M. Harris, 1983: A determination of the absolute radiant energy of a Robertson–Berger meter sunburn unit. *Atmos. Environ.*, **17,** 751–758.

Farman, J. C., B. G. Gardiner, and J. D. Shanklin, 1985: Large losses of total ozone in Antarctica reveal seasonal ClO_x/NO_x interaction. *Nature,* **315,** 207–210.

Green, A. E. S., T. Sawada, and E. P. Shettle, 1974: The middle ultraviolet reaching the ground. *Photochem. Photobiol.*, **20,** 251–259.

Parrish, J. A., K. F. Jaenicke, and R. R. Anderson, 1982: Erythema and melanognesis action spectra of normal human skin. *Photochem. Photobiol.*, **36,** 187–191.

Robertson, D. F., 1972: Solar ultraviolet radiation in relation to human sunburn and skin cancer. Ph.D. thesis, University of Queensland, Australia, 131 pp.

Scotto, J., and T. R. Fears, 1977: Intensity patterns of solar ultraviolet radiation. *Environ. Res.*, **14,** 113–127.